

A Unified Framework for N -Dimensional Visualization and Simulation: Implementation and Evaluation including 4D Boolean Operations

Hirohito Arai
Ritsumeikan Uji High School

December 2025

Abstract

This study proposes a unified framework for simulation and visualization of intuitive exploration of phenomena in N -dimensional space. While specialized libraries offer powerful geometric algorithms, they typically lack integrated environments for interactive trial and error, creating a barrier for researchers. The contribution of this research is the integration of Quickhull-based mesh generation, visualization via hyperplane slicing, and computationally expensive Boolean operations into a single, extensible platform, while maintaining interactivity. To validate its effectiveness, this paper presents a 4-dimensional implementation and introduces a new interaction design, termed ‘High-Dimensional FPS,’ to enable intuitive high-dimensional exploration. Furthermore, as a case study to demonstrate the framework’s high extensibility, I also integrated a non-rigid body physics simulation based on Extended Position Based Dynamics (XPBD). Experimental results confirmed the effectiveness of the proposed method, achieving real-time rendering (80 fps) of complex 4D objects and completing Boolean operations within seconds in a standard PC environment. By providing an accessible and interactive platform, this work lowers the entry barrier for high-dimensional simulation research and enhances its potential for applications in education and entertainment.

1 Introduction

While the simulation and visualization of high-dimensional spaces are theoretically established to some extent, practical integrated environments and concrete methods are limited. This study proposes a unified framework for N -dimensional simulation and visualization that can be easily adopted and applied by researchers and developers. This framework unifies previously disparate techniques—such as Quickhull-based high-dimensional convex hull mesh generation, visualization based on hyperplane slicing, high-dimensional exploration through view transformations, and mesh processing via Boolean operations—enabling their integrated use and providing an environment for the intuitive understanding of high dimensions.

Previously, functionalities such as high-dimensional mesh generation and Boolean operations were offered within specialized computational geometry libraries like the Computational Geometry Algorithms Library (CGAL). However, an environment that combined these with visualization and physics simulation to enable interactive trial and error has been lacking.

The framework proposed in this paper is positioned as one solution to this challenge. Its architecture, founded on the design principle of separating topology and geometry, achieves high extensibility. I demonstrate its effectiveness through a case study integrating a non-rigid body physics simulation based on Extended Position Based Dynamics (XPBD), showing that external components can be easily integrated. This approach is expected to lower

the barrier to entry for high-dimensional simulation research, enhance its potential for applications in education and entertainment, and contribute to the future growth of the research community and academic advancement.

2 Related Work

Prior research in high-dimensional simulation and visualization has primarily focused on reporting individual techniques. In mesh generation, the construction of convex hull meshes using the Quickhull algorithm is widely known [2], but it has a high computational cost to guarantee mathematical rigor. In physics simulation, while simulations of non-rigid bodies based on XPBD have been reported for 3D space [4], and research on the simulation of rigid bodies in 4D and higher dimensions exists [6], there are exceedingly few reports of integrated environments that allow for the interactive manipulation of non-rigid bodies and the visualization of objects in 4D or higher dimensions. Turning to mesh editing, Boolean operations are a standard technique in 3D. In higher-dimensional spaces, specialized computational geometry libraries like CGAL also provide this functionality as an offline computation. However, these processes require significant computational resources to guarantee mathematical precision and are not intended for interactive use that involves real-time result verification. Regarding visualization, while a GPU-based 4D visualization architecture has been proposed [3], its primary focus is on fast rendering, and it offers a limited environment for the kind of exploratory experience that this paper aims to achieve.

3 Proposed Method

3.1 Design Philosophy and Architectural Overview

This section describes the technical details of the proposed unified framework. This framework integrates the functionalities of mesh generation, Boolean operations, visualization, and physics simulation into a single, extensibility-focused pipeline. I will first provide an overview of the entire architecture, and then detail the

core algorithms that constitute each function and their implementation.

In the design and implementation of this framework, three principles were emphasized: algorithmic transparency, minimal reliance on external libraries, and future extensibility. This is a design decision that prioritizes the framework’s utility as a research platform—allowing researchers to easily understand, verify, and incorporate new functionalities into the high-dimensional geometry algorithms—over extreme performance optimization. Based on this philosophy, all computational geometry logic is unified in a standard C# implementation on the CPU. While GPU-based parallelization can deliver high performance for specific tasks, it introduces issues of code complexity and hardware dependency. The CPU-centric approach of this paper aims to enhance platform independence and algorithmic transparency. This implementation strategy is expected to lower the technical barriers for other researchers to verify this study’s algorithms or apply them to their own research. Furthermore, within the scope of this paper, numerical robustness related to floating-point arithmetic is excluded from consideration and is left for future work. The software for this research was implemented in C# on the Unity engine and is available as an open-source project [1].

3.2 Overview of the Overall Architecture

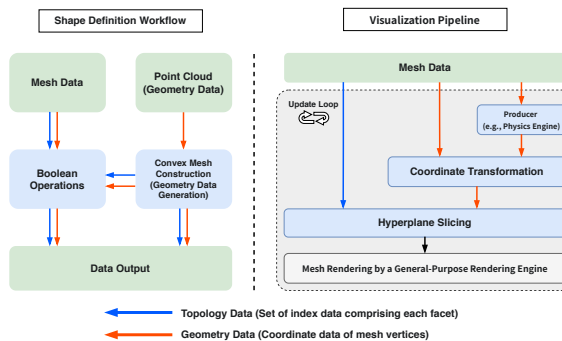


Figure 1: An overview of the proposed framework. The left side shows the static shape definition workflow, and the right side shows the dynamic visualization pipeline.

As illustrated in Figure 1, the overall architecture and

data flow of this framework consist of multiple loosely coupled components: convex hull mesh generation, mesh editing, and visualization. The mesh generation component uses a Quickhull-based algorithm to construct an index list of facets from the input point cloud data, which defines the topology of the N -dimensional object. The mesh editing component dynamically processes and modifies the mesh’s topology and geometry based on user operations, such as Boolean operations. The visualization component generates and renders a 3D cross-section each frame by performing hyperplane slicing on the coordinate-transformed mesh, based on the current vertex coordinates and the user’s viewpoint.

Each component interacts only through a well-defined data structure for the object’s topology and geometry, thereby ensuring high modularity. Furthermore, I have adopted Geometric Algebra as a unified mathematical foundation that enables the consistent handling of geometric entities such as N -dimensional vectors, planes, and rotations. For Geometric Algebra itself, which I use as my foundation, [7] is cited as an excellent introductory text for researchers in computer graphics.

3.3 N-Dimensional Convex Hull Construction

3.3.1 Comparison with Existing Methods

This component is centered around a self-contained C# implementation of the classic N -dimensional Quickhull algorithm [2]. A standard implementation would perform an optimization called candidate point pruning to maximize computational efficiency. This strategy, in which each facet individually manages a list of candidate points and excludes points absorbed into the convex hull’s interior from computation, is extremely effective for volumetric point clouds containing numerous interior points. However, the primary applications within my framework—such as the basic convex hull mesh construction for initial shapes and dynamic simplicial tessellation (detailed in Section 3.3.3)—involve frequently handling small-scale, surface-like point clouds, typically with fewer than several dozen vertices and almost no interior points. In such contexts, the performance gain offered by a pruning mechanism is limited, while the added implementation complexity reduces code maintainability

and introduces risks to robustness in a floating-point arithmetic environment.

Therefore, my implementation considers this trade-off and intentionally omits the pruning mechanism. As shown in Figure 2, my algorithm performs a linear search over a single, global set of unprocessed points to find the farthest point, and removes only those points that are used as vertices of the convex hull from the set. This simplified state-management approach, in exchange for theoretical computational efficiency on large volumetric point clouds, provides the practically significant advantages of implementation simplicity and independence from external libraries for my primary use cases. Hereafter in this paper, I will refer to this method as “Direct Quickhull.”

3.3.2 Calculating N-Dimensional Normals and Visible Facets

In Direct Quickhull, efficiently computing facet normal vectors plays a crucial role in determining overall performance. The conventional approach based on null-space computation is unsuitable for real-time applications, as it typically requires methods such as Singular Value Decomposition (SVD). To solve this problem, my implementation introduces the concepts of the wedge product and the dual from Geometric Algebra. First, in an N -dimensional space \mathbb{R}^N , I define a facet from its N vertices $\{\mathbf{p}_0, \mathbf{p}_1, \dots, \mathbf{p}_{N-1}\}$ and construct the $(N - 1)$ linearly independent vectors that span the facet.

$$\mathbf{v}_i = \mathbf{p}_i - \mathbf{p}_0 \quad (\text{for } i = 1, \dots, N - 1) \quad (1)$$

Next, I calculate the wedge product of these vectors.

$$\mathbf{B} = \mathbf{v}_1 \wedge \mathbf{v}_2 \wedge \dots \wedge \mathbf{v}_{N-1} \quad (2)$$

In Geometric Algebra, this $(N - 1)$ blade \mathbf{B} is a mathematical entity that represents the oriented hyperplane spanned by the vectors. The operation of taking the Hodge dual of this blade, \mathbf{B}^* , is equivalent to finding the orthogonal complement of that hyperplane. That is, for an $(N - 1)$ -dimensional hyperplane, its orthogonal complement is a 1-dimensional line, and its direction vector becomes the normal vector \mathbf{n} to the hyperplane.

$$\mathbf{n} = \mathbf{B}^* \quad (3)$$

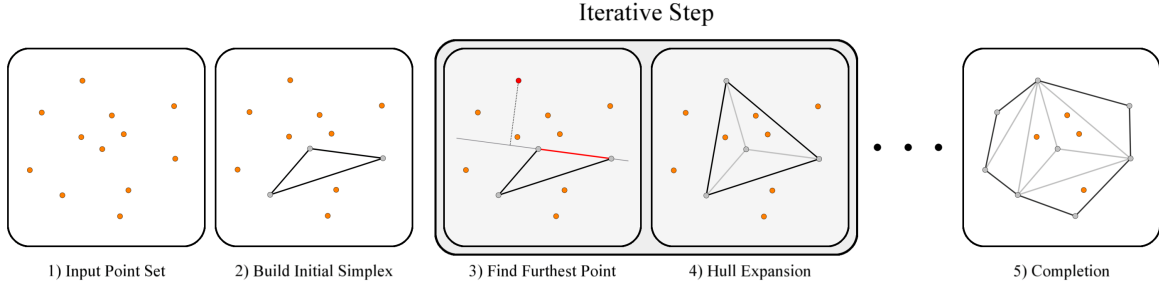


Figure 2: Stages of vertex management and convex hull construction in Direct Quickhull. Orange vertices are unprocessed, gray vertices are processed, gray facets are interior, and black facets form the outer hull. In the iterative step, the convex hull is expanded using a selected facet from the hull (red) and its farthest point (red).

This series of operations can ultimately be implemented efficiently as the calculation of the determinant of an $n \times n$ matrix, as follows:

$$\mathbf{n} := \det \begin{vmatrix} \mathbf{e}_1 & \mathbf{e}_2 & \dots & \mathbf{e}_n \\ v_{1,1} & v_{1,2} & \dots & v_{1,n} \\ v_{2,1} & v_{2,2} & \dots & v_{2,n} \\ \vdots & \vdots & \ddots & \vdots \\ v_{n-1,1} & v_{n-1,2} & \dots & v_{n-1,n} \end{vmatrix} \quad (4)$$

Next, it is necessary to correctly determine the orientation of the facet's normal vector. In conventional 3D, the correct orientation of a normal vector for a facet on the surface of a convex hull was obtained by computing the vertex winding order, which relies on the right-handed rule of the cross product. However, the cross product is unique to 3D space. In higher dimensions, there are no geometric concepts analogous to the winding order that intuitively define a face's orientation.

To solve this problem, my implementation uses the geometric property that the normal vectors of a convex hull's facets must always point outward. This orientation is determined by calculating the dot product of the facet's normal vector and a vector pointing from a point on the facet to the centroid of the initial simplex constructed at the beginning of the algorithm. If the sign of the dot product is negative, the normal vector is determined to be pointing outward. If the sign is positive, its sign is inverted, thereby ensuring that I always obtain a normal vector with the correct outward-facing orientation.

Next, I use the facet normal vectors to determine the

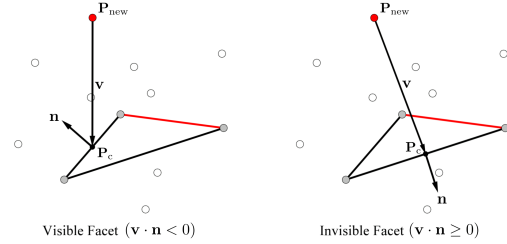


Figure 3: The logic for determining visible facets in Quickhull. This illustrates the method for identifying facets that are visible from the farthest point \mathbf{P}_{new} . The centroid of the facet being tested is denoted as \mathbf{P}_c , and its normal vector is \mathbf{n} . The vector pointing from \mathbf{P}_{new} to \mathbf{P}_c is defined as \mathbf{v} .

visible facets, which is a necessary step in the process of expanding the convex hull.

As shown in Figure 3, the facets visible from \mathbf{P}_{new} can be found by examining the sign of the dot product of \mathbf{v} and \mathbf{n} . The convex hull can then be expanded by connecting the new vertex \mathbf{P}_{new} to the boundary of the identified set of visible facets (i.e., the set of ridges that are not shared among the visible facets).

3.3.3 Method for Simplicial Tessellation during Convex Hull Construction

my implementation not only computes the facets that constitute the surface of the convex hull but is also equipped

with the functionality to simultaneously generate its interior volume as a set of N -dimensional simplices. This is accomplished by applying the incremental process of the Quickhull algorithm. In Quickhull’s incremental process, the newly added volume is represented as a set of N -dimensional simplices formed from the new vertex \mathbf{p}_{new} and the visible facets. My implementation directly uses this principle, appending the corresponding simplices to a list. By repeating this process, I simultaneously obtain both the surface facets of the convex hull and a list of simplices that perfectly tessellates its interior volume. This simplicial decomposition data serves two important roles within this framework. Its primary application is to serve as the base data for rapidly performing a simplicial decomposition of the interior of facets clipped during Boolean operations. Furthermore, it is intended for future application in efficiently determining the cross-sectional structure of facets from hyperplane slicing in spaces of five or more dimensions, a topic detailed in Section 3.5.3.

3.4 N-Dimensional Boolean Operations

3.4.1 Algorithm Overview and Design Philosophy

While Boolean operations are an extremely powerful method for interactively modifying the shape of an N -dimensional mesh, their interactive implementation in high-dimensional space presents a significant challenge from a computational cost perspective. To address this challenge, my framework implements a practical four-stage algorithm. First, in a broad phase, I use spatial partitioning to narrow down potential intersection candidates. Next, in a narrow phase, I determine the actual geometric intersections. The intersected facets are then decomposed into smaller facets in a tessellation stage. Finally, the results are classified in an inside-outside test stage to construct the final operation result.

In designing this algorithm, I prioritized a balance of three factors over extreme performance optimization or a full guarantee of mathematical rigor: implementation simplicity, extensibility to N -dimensions, and a practical level of performance that enables interactive trial and error. The following sections will detail the specific techniques used in each stage and the design decisions behind them.

3.4.2 Broad Phase: Candidate Pruning via Spatial Partitioning

In N -dimensional Boolean operations, a brute-force intersection test between all facets of two meshes, with N_A and N_B facets respectively, has a computational complexity of $O(N_A N_B)$, making it a major bottleneck in interactive implementations. To avoid this problem, my implementation introduces a spatial partitioning grid as the broad phase to efficiently prune pairs of facets that could potentially intersect. I compute the axis-aligned bounding box (AABB) for each facet and register the facet with the grid cells that its AABB occupies. As a result, only facet pairs that share a common cell become candidates for the precise intersection tests in the subsequent narrow phase. Compared to hierarchical spatial partitioning methods such as BVH or Octree, the uniform grid approach adopted in my implementation offers the advantage of being simple to implement while still achieving practical pruning performance for my target use cases.

3.4.3 Narrow Phase: Facet-Facet Intersection Test

In the narrow phase, I perform precise geometric intersection tests on the candidate pairs pruned during the broad phase. The principle of this algorithm is a generalization to N -dimensions of the method proposed by Tomas Möller et al. for fast triangle-triangle intersection tests in 3D [5]. Its essence lies in decomposing the intersection test between two facets, \mathcal{F}_A and \mathcal{F}_B , into two symmetric sub-problems. First, I compute the geometric intersection region, \mathcal{I}_B , between the $(N - 1)$ -dimensional hyperplane spanned by \mathcal{F}_A and the facet \mathcal{F}_B . Second, I perform the same operation with the roles swapped, computing the intersection region \mathcal{I}_A between the hyperplane spanned by \mathcal{F}_B and the facet \mathcal{F}_A . Both of these intersection regions are $(N - 2)$ -dimensional convex polytopes. Finally, I determine if an intersection between the facets exists by testing whether \mathcal{I}_A and \mathcal{I}_B overlap within their common $(N - 2)$ -dimensional space.

If an intersection is found to exist, this information is utilized in the subsequent tessellation stage. Specifically, I register this intersection pair in a dictionary where one facet is the key and the other is the value. By performing this process for all intersection pairs, I can systematically construct information about the clipping relationships, en-

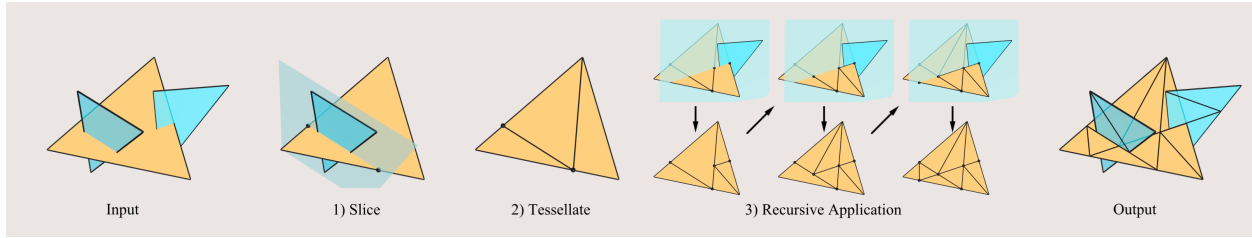


Figure 4: The sequential tessellation process of a facet in a Boolean operation (analogized in 3D). After the input facet (yellow) is clipped and tessellated by a facet from the opposing object (blue, left), each resulting facet is further tessellated by a subsequent blue facet, as shown in the center. By repeating this process for all intersecting facets, a mesh (Output) that is accurately partitioned at the boundary with the opposing object is ultimately generated.

abling us to handle complex situations where one facet intersects with multiple other facets.

In my 4D implementation, the intersection region is a 2D convex polygon. Since the number of vertices is small, I adopted the Separating Axis Theorem (SAT), which is relatively straightforward to implement. However, in five or more dimensions, the maximum number of vertices of the $(N - 2)$ -dimensional polytope intersection region increases, making the implementation of SAT more complex. Therefore, for extension to higher dimensions, an intersection test approach using the GJK algorithm is considered a more practical option.

3.4.4 Dynamic Tessellation via Direct Quickhull

A facet that is found to intersect in the narrow phase is clipped by the $(N - 1)$ -dimensional hyperplane spanned by the opposing facet, and the clipped facet is then tessellated into multiple smaller facets. This entire process is illustrated in Figure 4 using an analogy in 3D. As the figure shows, clipping can decompose the original facet, an $(N - 1)$ -dimensional simplex, into an $(N - 1)$ -dimensional convex polytope with more than N vertices. Consequently, it is necessary to efficiently re-tessellate the resulting polytope back into multiple smaller facets.

The core of this tessellation algorithm is to classify the vertices of the facet into the positive side (P-side) and the negative side (N-side) based on their position relative to the clipping hyperplane. The tessellation process is executed only when the facet has vertices in both half-spaces; otherwise, no tessellation is performed.

However, in an implementation that assumes floating-

point arithmetic, this theoretical classification alone is insufficient. Problems can arise from numerical errors, such as an intersection that should theoretically be a single point being detected as multiple points, or the classification becoming unstable when a vertex is extremely close to the hyperplane. To address this challenge, my implementation introduces a two-stage vertex merging process. First, it unifies points that are in close proximity to each other within the computed set of intersection vertices. Second, it evaluates the distance between each vertex of the merged intersection region and the vertices of the original facet; if they are close, the intersection vertex is completely snapped to the coordinates of the facet vertex. While this operation may introduce minor deformations to the mesh geometry, it plays a crucial role in maintaining the topological consistency of the original facet within the tessellated mesh.

After the merging process, the final tessellation is performed. First, I apply the simplicial tessellation feature of Direct Quickhull to the combined surface-like point cloud of the P-side vertices and the intersection region vertices to tessellate the P-side region into multiple smaller facets. Next, a similar operation is performed for the N-side vertices and the intersection region vertices to tessellate the N-side region. Through these two processes, the original facet is tessellated such that its mesh structure is consistent with the clipping plane. This approach demonstrates that Direct Quickhull can effectively use its capabilities even in dynamic mesh processing, thereby guaranteeing the N -dimensional extensibility of the entire algorithm.

3.4.5 Inside-Outside Testing and Result Construction

To construct the final result of a Boolean operation—namely, the union, intersection, or difference from the set of tessellated facets, it is necessary to classify whether each facet is inside or outside the opposing object. For this inside-outside test, my implementation adopts the ray casting method. The fundamental principle of this method is based on intersection parity. A ray is cast from the centroid of the facet under test toward the opposing surface, and the number of intersections is counted. The state is then determined according to whether this number is even or odd, and the same logic applies in N -dimensional space. In my implementation, the ray is parallel to the x -axis, and its endpoint is set to a point slightly beyond the opposing mesh's AABB. This ensures both computational efficiency and stability. To make this method operate robustly in a floating-point environment, it is necessary to handle degenerate cases where the ray passes through a facet's vertices or edges, as shown in Figure 6. In an implementation that introduces a tolerance, an intersection with a vertex or edge, which should theoretically be a single point of intersection, can be detected as multiple, slightly different intersection points with the various facets that share that feature. This disrupts the parity of the intersection count and causes the inside-outside test to fail. To prevent this misclassification, my implementation employs a two-stage solution. First, the coordinates of the detected intersection points are discretized based on a tolerance, and multiple proximate intersection points are grouped into a single 'intersection event' so they can be handled uniformly in subsequent processing. Next, the nature of this grouped intersection event is determined. Specifically, it is necessary to distinguish whether the ray is piercing the surface or merely touching it.

To do this, I evaluate the dot product of the ray's direction vector and the normal vector of every facet included in the event. If the signs of the dot products are biased to one side (either all positive or all negative), the event is considered to be piercing the surface, and the intersection count is incremented by one. If, on the other hand, the signs are distributed between both positive and negative, the ray is determined to be just tangent to the surface, and it is not included in the intersection count. Based

on this inside-outside test executed through this series of processes, the tessellated facets are classified according to the type of Boolean operation, and the final mesh is constructed.

However, in cases where the ray is coplanar with a facet, such as the "Co-planar Facet" case shown in Figure 5, the dot product of the ray and the normal vector is theoretically zero, causing the sign-based test to fail robustly. Therefore, there is no guarantee that intersections can always be correctly determined under these conditions. A practical approach would be to avoid such degenerate geometric configurations by using existing techniques, such as ray perturbation.

3.5 Visualization of N-Dimensional Objects

3.5.1 Cross-Sectioning as the Basic Strategy

This component is responsible for generating and rendering 3D cross-sections based on N -dimensional mesh data. The basic strategy to achieve this transformation is based on the concept of sequentially reducing the dimension. This is a process of recursively clipping an N -dimensional object with an $(N - 1)$ -dimensional hyperplane, and then clipping the resulting cross-section with an $(N - 2)$ -dimensional hyperplane. In this paper, I refer to this method of sequentially reducing dimensions as Hierarchical Cross-Sectioning. With this approach, the complex problem of computing cross-sections in arbitrary dimensions can always be reduced to the simpler problem of the intersection between an N -dimensional facet and an $(N - 1)$ -dimensional hyperplane. In the following sections, as a concrete application of this Hierarchical Cross-Sectioning for $N = 4$, I will detail the specific algorithm for generating 3D cross-sections from 4D objects and discuss its implementation challenges.

3.5.2 Facet Clipping Algorithm in the 4D Implementation

To generate a 3D cross-section of an object in 4D space, my implementation computes the geometric intersection between each facet of the 4D object—a tetrahedron—and an axis-parallel hyperplane $w = w_{\text{slice}}$ (where $w = w_{\text{slice}}$ is an arbitrary constant). This procedure is executed independently for every facet of the input mesh according to

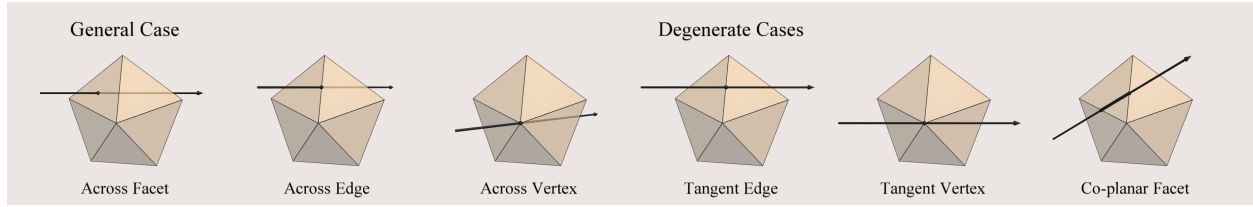


Figure 5: Classification of general and degenerate intersection cases. This figure categorizes the general case, where a ray crosses a single facet, and representative degenerate cases that require precise intersection tests, where the ray passes exactly through a facet, edge, or vertex.

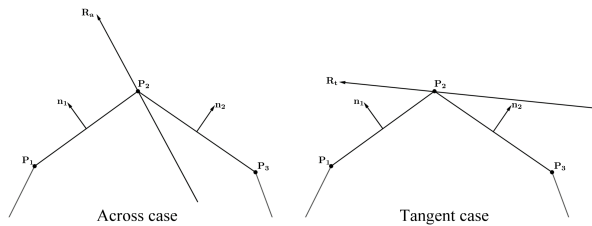


Figure 6: An example of a degenerate case in intersection testing. In the figure, \mathbf{P}_1 , \mathbf{P}_2 , and \mathbf{P}_3 are the vertices of a 2D polygon; \mathbf{n}_1 and \mathbf{n}_2 are the outward-facing normal vectors of the edges connected to vertex \mathbf{P}_2 ; and \mathbf{R}_t and \mathbf{R}_a are two different rays passing through \mathbf{P}_2 . The left diagram shows a piercing case, and the right diagram shows a tangent case.

the following steps.

First, I determine on which side of the clipping hyperplane each of the facet's four vertices is located. If all vertices are on the same side, the facet does not intersect the hyperplane and skip intersection computation. If the vertices straddle the hyperplane, the intersection point of each constituent edge of the facet with the hyperplane is calculated via linear interpolation. Let the two vertices defining an edge be

$$\mathbf{p}_0 = (x_0, y_0, z_0, w_0) \quad \mathbf{p}_1 = (x_1, y_1, z_1, w_1) \quad (5)$$

The interpolation parameter t for determining the position of the intersection point is then calculated from the w -coordinates of both vertices and the w -coordinate of the clipping plane, w_{slice} , as shown in Equation (6).

$$t = \frac{w_{\text{slice}} - w_0}{w_1 - w_0} \quad (6)$$

Next, using this parameter t , the coordinates of the intersection point $\mathbf{p}_{\text{isect}}$ in 4D space are calculated according to Equation (7).

$$\mathbf{p}_{\text{isect}} = \mathbf{p}_1 + t(\mathbf{p}_1 - \mathbf{p}_0) \quad (7)$$

The 3D coordinates, obtained by extracting the x, y, z components of the resulting 4D coordinate vector $\mathbf{p}_{\text{isect}}$, directly become the coordinates of a vertex that constitutes the cross-section.

By performing this operation for all edges that intersect the hyperplane, I obtain the set of vertices of the cross-section, which are then connected to form a polygon. The shape of the cross-section generated by the intersection of a single 4D facet and a 3D hyperplane is, within 3D space, either a triangle with three vertices or a convex polygon with four vertices. A 4-vertex convex polygon can be divided into two triangles to obtain a set of triangular polygons for rendering.

3.5.3 Simplicial Decomposition of the Cross-Section

The cross-section generated by the above clipping algorithm is generally an $(N - 2)$ -dimensional convex polytope. For subsequent processing, this must be decomposed into a set of $(N - 2)$ -dimensional simplices. In the 4D implementation, the cross-section is a 2D convex polygon (either a triangle or a quadrilateral) with a maximum of four vertices, as shown in Figure 7. Although the order of the vertex list is undefined, the polygon can be safely tessellate into two triangles by sorting the vertices by angle around the polygon's centroid and then sys-

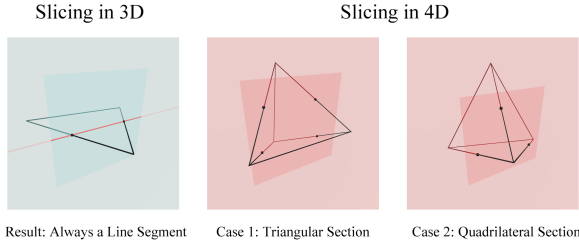


Figure 7: Dimensional dependence of the number of cross-section vertices generated during hyperplane clipping. When clipping a facet in 3D, the number of vertices is always two. However, when clipping a 3D facet in 4D, the number varies between three and four depending on the relative position of the hyperplane, and is thus not uniquely determined. Regarding the color coding in this figure, the blue plane represents the clipping hyperplane, and the red area indicates the portion of it that exists on the dimension being clipped. The darker shades are highlights for visual clarity.

tematically partitioning it. my implementation efficiently performs this sort using only vector operations, avoiding computationally expensive trigonometric functions.

However, this angle-sorting method cannot be generalized to five or more dimensions ($N \geq 5$). The maximum number of vertices of an $(N-2)$ -dimensional cross-section, obtained by clipping an N -dimensional facet (which has N vertices) with a hyperplane, is given by the well-known result in combinatorics shown in Equation (8).

$$\left\lfloor \frac{N}{2} \right\rfloor \cdot \left\lceil \frac{N}{2} \right\rceil \quad (8)$$

For example, in 5D, the cross-section can be a 3D convex polytope with a maximum of $\lfloor 5/2 \rfloor \cdot \lceil 5/2 \rceil = 6$ vertices. The simplicial tessellation of such a complex polytope is a non-trivial computational problem. As a dimension-independent and general solution to this high-dimensional extensibility challenge, I can use the simplicial tessellation feature of Direct Quickhull, which was detailed in Section 3.3.3. By providing the set of vertices that constitute the cross-section as input to Direct Quickhull, it is possible to efficiently tessellate the interior of the cross-sectional polytope itself into a set of $(N-1)$ -

dimensional facets. As mentioned in Section 3.3.1, my implementation, which omits the interior point search, is well-suited for processing this type of surface-like point cloud. This ensures that the visualization pipeline of my framework is, in principle, extensible to higher dimensions.

3.5.4 Robust Method for Determining Cross-Section Normals

When generating a 3D cross-section for rendering from a 4D object, it is necessary to determine the winding order of the vertices that form the 3D facet. The clipping algorithm from the previous section produces a list of vertices in an undefined order. If this unordered vertex list is used as is, a serious problem arises: many rendering pipelines determine the front and back of a face based on the input order, which would result in inconsistent face orientations and prevent the correct rendering of the shape.

To solve this problem, my method utilizes the normal vector of the original 4D facet as a reference for the correct orientation. Specifically, I first project the original 4D normal vector into 3D space by extracting its x, y, z components, and define this as the true normal vector that the 3D facets should follow. Next, I compute a temporary normal vector from the generated vertex set using the cross product and evaluate its dot product with the true normal vector. If the sign of this dot product is negative, the winding order of the vertices is reversed. This ensures that all triangles constituting the cross-sectional mesh have a consistent vertex winding order that can be correctly interpreted by a general-purpose renderer.

3.6 Pose Representation and Control Scheme for Interactive Exploration

3.6.1 Pose Representation and Management with Geometric Algebra Rotors

In representing the pose of an N -dimensional object, conventional 3D methods like Euler angles or quaternions cannot be directly applied due to issues such as gimbal lock and difficulties in extending them to higher dimensions. To solve this challenge, my framework adheres to the mathematical foundation of Geometric Algebra, as

mentioned in Section 3.2, and represents the object’s pose uniformly using a Rotor.

A rotor is a rotation operator defined by a specific plane of rotation and a rotation angle, which allows the composition of rotations and their application to vectors to be handled as an algebraic product, regardless of the dimension. A bivector \mathbf{B} representing the plane of rotation is parallel to the plane spanned by two vectors, \mathbf{a} and \mathbf{b} , and can be defined by their wedge product:

$$\mathbf{B} = \mathbf{a} \wedge \mathbf{b} \quad (9)$$

A rotor is an operator that represents a rotation of an arbitrary angle with respect to this plane. The rotor R is defined using the normalized bivector $\hat{\mathbf{B}}$ as follows:

$$R = \cos \frac{\theta}{2} + \sin \frac{\theta}{2} \hat{\mathbf{B}} \quad (10)$$

The rotation of a vector is then expressed using the rotor as shown in the following equation:

$$\mathbf{v}' = R\mathbf{v}\tilde{R} \quad (11)$$

Here, \tilde{R} is the reverse of the rotor R . If R is normalized, \tilde{R} is equivalent to R^{-1} .

In my implementation, instead of having the user manipulate the rotor directly, I allow them to specify the amount of rotation for each of the six fundamental rotation planes in 4D space (xy, xz, xw, yz, yw, zw) as individual parameters, similar to Euler angles. These parameter values are then composed in a predefined order to internally construct the final rotation operator, the rotor. This design, which separates the intuitive parameters provided to the user from the mathematically robust operator used internally, completely avoids gimbal lock and is easily extensible to higher dimensions. Furthermore, my implementation fixes the clipping hyperplane to be axis-parallel ($w = \text{const}$) and transforms the object’s pose instead. From the user’s perspective, this approach is visually equivalent to clipping a stationary object with an arbitrarily oriented hyperplane. However, it replaces the computationally expensive problem of arbitrary hyperplane clipping with a combination of an efficient pose transformation and an axis-parallel clip, enabling interactive observation of the cross-sections.

3.6.2 Camera-Based Coordinate Transformation

This section defines the view transformation in N -dimensions, which transforms vertices from the world coordinate system to the camera coordinate system based on the camera’s state (position and pose).

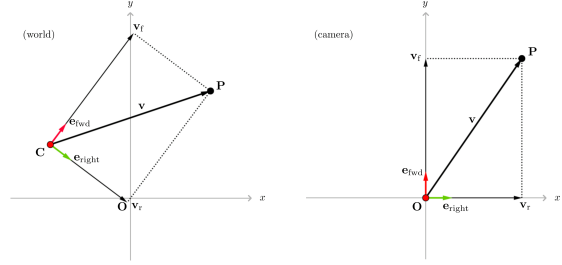


Figure 8: A conceptual diagram of the coordinate transformation from the world coordinate system to the camera coordinate system. Let the camera’s position be \mathbf{C} and the target point be \mathbf{P} . The relative position vector of the target point, \mathbf{v} , is defined as the difference between \mathbf{P} and \mathbf{C} . The components obtained by projecting \mathbf{v} onto the basis vectors that represent the camera’s orientation, $\mathbf{e}_{\text{right}}$ and \mathbf{e}_{fwd} , directly become the coordinate values of \mathbf{P} in the camera coordinate system. In this setup, the camera’s position \mathbf{C} corresponds to the origin of the camera coordinate system.

To intuitively understand the geometric essence of this transformation, I consider the 2D space shown in Figure 8 as an example. I denote the position of a target vertex \mathbf{P} in the world coordinate system as $\mathbf{P}^{(W)}$ and the position of the camera \mathbf{C} as $\mathbf{C}^{(W)}$. The coordinate transformation takes $\mathbf{P}^{(W)}$, $\mathbf{C}^{(W)}$, and the rotor R representing the pose as input. The transformation process first derives the basis vectors that span the camera coordinate system, $\mathbf{e}_{\text{right}}^{(W)}$ and $\mathbf{e}_{\text{fwd}}^{(W)}$, from the rotor R representing the camera’s pose, as shown in Equation (11). Next, the relative position vector $\mathbf{v}^{(W)}$ from the camera’s position to the object’s vertex is calculated as shown in Equation (12).

$$\mathbf{v}^{(W)} = \mathbf{P}^{(W)} - \mathbf{C}^{(W)} \quad (12)$$

Finally, this relative vector $\mathbf{v}^{(W)}$ is projected onto each basis vector via the dot product, and the resulting pro-

jection lengths determine the respective components of $\mathbf{P}^{(C)}$.

$$\begin{aligned} \mathbf{P}_x^{(C)} &= \mathbf{v}^{(W)} \cdot \mathbf{e}_{\text{right}}^{(W)} \\ \mathbf{P}_y^{(C)} &= \mathbf{v}^{(W)} \cdot \mathbf{e}_{\text{fwd}}^{(W)} \end{aligned} \quad (13)$$

This entire sequence of processes can be interpreted as two separate geometric operations. Equation (12) corresponds to a translation that aligns the origin of the world coordinate system with the camera’s position. Equation (13) corresponds to a rotation that aligns the coordinate system with the camera’s orientation. By using homogeneous coordinates, these two operations can be combined into a single $(N + 1) \times (N + 1)$ matrix, analogous to the view matrix commonly used in computer graphics. The description using dot products in this paper is specifically intended to directly illustrate the geometric meaning of the rotation operation.

3.6.3 Design of the Control Scheme for Interactive Exploration

To address the challenge of mapping the six independent rotational degrees of freedom required to control the camera’s orientation in 4D space onto a standard mouse and keyboard, I adopted two design principles: orthogonality of controls and leveraging existing control conventions (specifically, those of First-Person Shooters, or FPS). The 3D translations (WASD keys) and pitch rotation (mouse vertical movement) follow standard conventions. The primary challenge, which is the assignment of a rotation to the horizontal mouse movement (x -axis), is resolved by a modal input switch using a modifier key (Left Control). In its normal mode, horizontal mouse movement controls the primary yaw rotation (xz -plane) for 3D exploration. While the modifier key is held down, this input is switched to control the rotation in the xw -plane, which serves a similar role in 4D exploration. This design ensures that a single input always corresponds orthogonally to a single operation, resulting in a highly predictable control scheme that allows the user to operate while being clearly conscious of switching between 3D and 4D exploration modes.

3.6.4 Extension of the Manipulation System to N Dimensions

This design principle can be generalized to N -dimensions. I apply a systematic approach to address the rotational degrees of freedom in an N -dimensional space, which increase quadratically as $N(N - 1)/2$. First, translations and rotations within the 3D cross-section that the user directly observes are kept on the standard control scheme (WASD/mouse), regardless of the total number of dimensions. This provides the user with a consistently stable operational base. Next, for the remaining $(N(N - 1)/2) - 3$ rotations outside the observed space, I consider an approach that generalizes the design of my 4D implementation. Specifically, horizontal mouse movement is consistently assigned to rotations that occur outside the observed space; the user selects the target high-dimensional axis (w, u, \dots) via a combination of modifier keys, which in turn manipulates the corresponding rotation plane (xw, xu, \dots). Because this approach dedicates the primary rotational input to high-dimensional exploration while allowing the control scheme to be systematically extended, it is expected to provide a scalable foundation for exploring N -dimensional space while preserving control orthogonality.

3.7 Demonstration of Extensibility

The core of this framework’s extensibility lies in the design principle of separating topology and geometry. This section demonstrates the effectiveness of this design through a case study in which a 4D non-rigid body physics simulation is integrated.

A practical challenge in this integration is the mismatch of data formats. For computational efficiency, the physics simulation requires unique, non-duplicated vertex data. The rendering pipeline, on the other hand, requires duplicated vertex data to accommodate correct normals and UVs. The separated architecture of my framework resolves this discrepancy through index mapping. During initialization, the physics engine extracts the set of unique vertices from the rendering mesh’s geometry and builds a map, just once, that maintains the correspondence between the indices of the unique vertices and the indices of the original, duplicated vertices. During the simulation, computations are performed only on the set of unique ver-

tices. Then, in each frame, this map is used to efficiently update the entire vertex array for rendering.

This pattern—maintaining an internally optimized data format and converting it to the required format only during communication is a general solution for integrating any external component that requires a different data format, and is not limited to this case study. This demonstrates that the design principle of separating topology and geometry is what enables the high modularity and extensibility of my framework.

4 Plex: An N -Dimensional Mesh Data Exchange Ecosystem

The N -dimensional simulation environments targeted by this research require, as their foundation, an extensible data exchange ecosystem for uniformly handling high-dimensional mesh data. However, to date, no widely accepted standard format for exchanging N -dimensional mesh data has existed, leading to a fragmented situation where formats vary among researchers and projects. This state of affairs has been a barrier to the smooth sharing of data between different tools and research groups. To address this challenge, this study defines a systematic data exchange ecosystem for N -dimensional meshes, named "Plex" (with the .plex extension), which is a file format featuring a chunk-based architecture.

4.1 Dual-Format Strategy

Research workflows that handle N -dimensional data present two distinct requirements: the need to inspect and verify data content in the early stages, and the need for high processing performance in large-scale computations. To meet these requirements, Plex adopts a dual-format strategy, following the design philosophy proven by the glTF format in the 3D domain.

The first format is a schema based on the standard JSON technology, which prioritizes data readability. This allows for the easy inspection and debugging of data content using a rich ecosystem of existing tools. The second is a chunk-based binary format, .plex, which prioritizes execution performance. This format is intended for fast loading by applications and efficient data storage.

The reference implementation provided in this study includes a one-way converter from the .plex format to the JSON format. This enables researchers to typically work with the high-performance binary format while exporting to a human-readable format as needed, thereby achieving a balance between execution efficiency and data transparency.

4.2 .plex Binary Format Specification

The .plex format is designed with a chunk-based architecture, following the proven extensibility model of standard formats such as PNG. A file consists of a global header followed by a sequence of at least four self-descriptive chunks as shown in Table 1; the internal structure of the META chunk is detailed in Table 2. Each chunk contains a 4-character chunk type, the data length, the data payload, and a CRC32 checksum to verify data integrity. The data payload structure for the primary chunks, excluding the META chunk, is defined as follows. The payload of the FACE chunk, which defines the topology, first specifies the total number of facets as a 64-bit unsigned integer, followed by a list of vertex indices (an array of 32-bit unsigned integers) that constitute each facet. In contrast, the payload for the VERT or VERD chunks, which store vertex coordinates, contains no metadata such as counts; for a mesh with V vertices in N dimensions, it consists solely of a contiguous array of $V \times N$ numerical values. The respective data types are 32-bit single-precision and 64-bit double-precision floating-point numbers. The payload layout for the NORM/NRMD chunks (storing facet normals) and the optional CENT/CNTD chunks (storing centroids) also conforms to this VERT/VERD chunk format.

A parser compliant with the specification is guaranteed to safely skip any unknown chunk types it cannot interpret. This ensures that backward compatibility with existing software is maintained even if the community adds new data in the future, such as textures or animations, as custom chunks.

Furthermore, to encourage community-driven extensions, a naming convention is established that reserves identifiers containing one or more lowercase letters for use as custom chunks. This standardization will facilitate data sharing among researchers and serve as a technical foundation for improving the reproducibility of published results. Moreover, the forward compatibility guar-

Table 1: Overview of standard chunks in the .plex format

Chunk Type	Requirement	Description
'META'	Required	Stores metadata for the entire mesh, such as the number of dimensions and vertices.
'VERT'/'VERD'	Required	Stores the geometry data of vertex coordinates in single or double precision.
'FACE'	Required	Stores the vertex indices (topology) that constitute the facets.
'NORM'/'NORMD'	Required	Stores the normal vectors that define the orientation of the facets in single or double precision.
'CENT'/'CENTD'	Optional	Stores the cached centroid coordinates of facets to reduce computational load.

Table 2: Internal data layout of the 'META' chunk

Offset	Size	Type	Description
0x00	4 bytes	int32	Dimension: N
0x04	4 bytes	uint32	Reserved: Padded with 0.
0x08	8 bytes	uint64	Vertex Count: V
0x10	8 bytes	uint64	Creation Time: Unix Time Stamp
0x18	8 bytes	uint64	Modified Time: Unix Time Stamp
0x20	1 byte	uint8	Precision Flag: 0=single precision, 1=double precision
0x21	3 bytes	byte[3]	Reserved: Padded with 0.
0x24	4 bytes	uint32	LSoftware: Byte length of the following software name.
0x28	Variable	char[]	Software Name: UTF-8 encoded string.

anted by this specification allows for future extensions, providing a sustainable infrastructure that transforms N -dimensional mesh data from something previously confined to individual environments into a resource that can be shared and reused by the entire community.

5 Experiments and Evaluation

5.1 Experimental Setup

The performance evaluation in this section is not intended to be a speed comparison with existing offline methods. Instead, its purpose is to evaluate the performance scalability of the proposed CPU-based framework with respect to the scale of the processed mesh (e.g., the number of facets). All implementation and performance evaluations in this study were conducted in the following environment.

Hardware Environment:

- **CPU:** Intel Core i7-12700H (2.30 GHz, 14Cores)
- **Memory:** 16 GB RAM

- **GPU:** Intel Iris Xe Graphics (Integrated, Shared Memory)

Software Environment:

- **OS:** Windows 11 Home (64-bit)
- **Development Environment:** Unity 2022.3 LTS (2022.3.62f2)
- **Programming Language:** C#

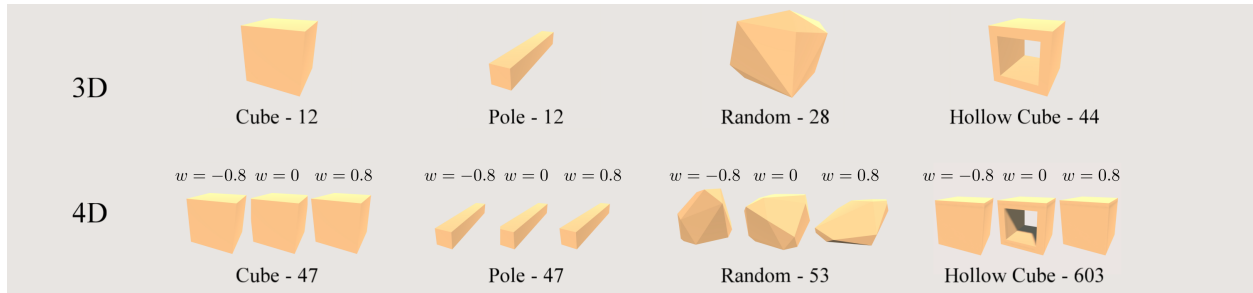


Figure 9: The set of base objects used in the experiments. The top row shows the 3D objects, and the bottom row shows the 4D objects. The number to the right of each object’s name is the number of facets that constitute its mesh. The 4D objects are visualized using the hyperplane slicing feature of my framework, with their 3D cross-sections at three representative w -coordinates ($w = -0.8, 0, 0.8$) displayed side-by-side.

5.2 Algorithmic Performance Evaluation

Table 3: Performance evaluation of the Direct Quickhull implementation. This table shows the average processing time for convex hull construction with randomly placed vertices (vertex count: 10 to 1000) in 3D and 4D spaces. The processing time is the average of 100 trials.

Dimension	Vertices	Time (ms)	Avg. Facets
3D	10	0.05	13.52
3D	20	0.12	25.32
3D	50	0.35	48.20
3D	100	0.88	73.34
3D	200	2.50	110.66
3D	500	9.43	185.24
3D	1000	26.95	268.32
4D	10	0.21	20.38
4D	20	0.56	43.11
4D	50	1.64	100.02
4D	100	3.84	174.32
4D	200	7.97	275.43
4D	500	27.43	496.94
4D	1000	75.99	779.91

5.2.1 Performance of the Direct Quickhull Implementation

As shown in Table 3, for small-scale point clouds with 50 or fewer vertices which are the intended primary use case in my framework the processing time is under 1.7 ms in either dimension, confirming that its performance is sufficient for this purpose.

5.2.2 Performance of N-Dimensional Boolean Operations

Next, I evaluated the performance of the N -dimensional Boolean operations, which are central to interactive mesh editing. I executed union, intersection, and difference operations between various objects in 3D and 4D spaces and measured their computation times. The results are presented in Table 4. In 3D space, the operations were generally completed in several tens of milliseconds, depending on the combination of objects and the type of operation. In 4D space, however, the computational load increased significantly. Even a simple combination of two Cubes required approximately 300 ms, and in some cases, operations between two complex Random objects took over two seconds to complete. These results indicate that high-dimensional Boolean operations can be executed on a time scale of a few seconds. This processing time is considered to be within an acceptable range for an interactive workflow, where the user waits for the result of an operation before considering the next action. This demonstrates the feasibility of incorporating these operations, which were previously dominated by offline batch processing, into interactive applications.

5.3 Interactive Performance Evaluation

This section quantitatively evaluates the performance characteristics of the proposed framework. I placed multiple simple 4D objects, each with 47 facets, and mea-

Table 4: Performance evaluation results for Boolean operations. I performed union, intersection, and difference operations in 3D and 4D spaces using combinations of the base objects shown in Figure 9. For each combination, the table shows the processing time and the size (number of facets) of the resulting mesh. The processing time is the average of three trials.

Input			Union		Intersection		Difference	
Dimension	ObjA	ObjB	Time (ms)	Size	Time (ms)	Size	Time (ms)	Size
3D	Cube	Cube	15.42	50	13.47	26	14.47	38
3D	Cube	Pole	11.55	56	10.62	24	12.43	36
3D	Cube	Random	20.87	87	18.60	59	20.46	79
3D	Cube	Hollow Cube	14.49	104	11.82	28	14.65	88
3D	Pole	Pole	13.75	64	11.46	32	10.95	48
3D	Pole	Random	25.39	86	20.78	38	19.72	74
3D	Pole	Hollow Cube	16.90	156	12.86	84	18.29	144
3D	Random	Random	33.65	98	28.24	54	24.50	78
3D	Random	Hollow Cube	21.56	126	20.94	56	17.82	94
3D	Hollow Cube	Hollow Cube	18.93	170	14.92	66	14.97	118
4D	Cube	Cube	323.44	1023	291.94	301	333.86	694
4D	Cube	Pole	205.06	768	186.23	299	176.74	324
4D	Cube	Random	2091.09	6142	2081.24	3777	2079.20	4143
4D	Cube	Hollow Cube	682.97	3017	656.85	1471	661.75	2693
4D	Pole	Pole	139.65	857	128.59	480	129.56	631
4D	Pole	Random	1225.35	2095	1213.80	1123	1237.35	1655
4D	Pole	Hollow Cube	638.94	3357	626.98	1353	639.27	3402
4D	Random	Random	2175.25	4449	2126.16	2326	2157.43	3114
4D	Random	Hollow Cube	2406.69	9633	2332.84	5292	2418.27	9181
4D	Hollow Cube	Hollow Cube	1598.95	7973	1559.87	4763	1576.44	6801

sured various performance metrics as the total number of facets in the scene was increased. The experimental results are shown in Table 5. These results indicate that the performance of my framework scales with the total number of facets in the scene. Furthermore, a specific performance limit was identified: the ability to maintain 30 fps, a common benchmark for interactive operation, is limited to a total facet count of approximately 500 (equivalent to about 10 objects). This measurement provides a performance baseline for evaluating the effects of future improvements, such as a GPU implementation.

6 Conclusion and Future Work

In this paper, I proposed an interactive framework for the unified simulation and visualization of N -dimensional space. The core of this framework lies in the design principle of separating topology and geometry. This allowed for the integration of functionalities such as

Quickhull-based mesh generation, hyperplane slicing, and N -dimensional Boolean operations onto a single platform. The effectiveness of this design was demonstrated through the integration of an XPBD-based physics simulation. I also proposed a control scheme for high-dimensional exploration and the Plex data exchange format.

The proposed algorithm can be extended to arbitrary dimensions; however, in this study, the evaluation was performed on the 4-dimensional implementation. Extension to five or more dimensions may introduce new performance bottlenecks due to the increased combinatorial complexity in intersection testing and tessellation. Furthermore, major future challenges include the development of a more robust N -dimensional non-rigid body model, application to new phenomena such as fluid simulations, and a GPU implementation of the parallelizable components currently handled by the CPU.

Table 5: Interactive performance evaluation. This table shows the rendering performance in scenes containing 1 to 20 4D objects (hypercubes with 47 facets each), while the user continuously performed movement and view rotation operations in the xz and xw planes for 30 seconds. Each value is the average of three 30 second measurement trials.

Objects (Total Facets)	Average FPS	Minimum FPS	99th Percentile Frametime (ms)
1(47)	77.9	29.8	19.9
5(235)	58.3	27.9	23.4
10(470)	38.6	16.8	32.5
15(705)	27.0	14.4	46.9
20(940)	21.2	13.1	58.1

Acknowledgments

I would like to express my sincere gratitude to Mr. Hiroaki Naito of Waseda Osaka High School for his constant and enthusiastic guidance throughout this research. I also wish to express my deepest appreciation to Professor Yasushi Homma of Waseda University for his valuable professional advice on the mathematical expressions related to Geometric Algebra used in this paper. Finally, I would like to thank the anonymous reviewers for their constructive comments, which helped to improve this manuscript.

- [5] Tomas Möller. A fast triangle-triangle intersection test. *Journal of Graphics Tools*, 2(2):25–30, 1997.
- [6] Marc Ten Bosch. N-dimensional rigid body dynamics. *ACM Transactions on Graphics (TOG)*, 39(4), 2020.
- [7] John Vince. *Geometric algebra for computer graphics*. Springer, 2008.

References

- [1] Hirohito Arai. A Unified Framework for N-Dimensional Visualization and Simulation. Version 1.0.0, <https://doi.org/10.5281/zenodo.17621258>, 11 2025.
- [2] C Bradford Barber, David P Dobkin, and Hannu Huuhdanpaa. The quickhull algorithm for convex hulls. *ACM Transactions on Mathematical Software (TOMS)*, 22(4):469–483, 1996.
- [3] Alan Chu, Chi-Wing Fu, Andrew Hanson, and Pheng-Ann Heng. Gl4d: A gpu-based architecture for interactive 4d visualization. *IEEE Transactions on Visualization and Computer Graphics*, 15(6):1587–1594, 2009.
- [4] Miles Macklin, Matthias Müller, and Nuttapong Chentanez. Xpbd: position-based simulation of compliant constrained dynamics. In *Proceedings of the 9th International Conference on Motion in Games*, pages 49–54, 2016.